

Efficient level-set segmentation model driven by the local GMM and split Bregman method

ISSN 1751-9659

Received on 19th September 2018

Revised 29th November 2018

Accepted on 6th January 2019

E-First on 20th March 2019

doi: 10.1049/iet-ipr.2018.6216

www.ietdl.org

Dengwei Wang¹ 

¹School of Aeronautics and Astronautics, University of Electronic Science and Technology of China, No. 2006, Xiyuan Ave, West Hi-Tech Zone, Chengdu 611731, People's Republic of China

✉ E-mail: wdengwei@126.com

Abstract: An efficient level-set model driven by the local Gaussian mixture model (GMM) and split Bregman method is proposed for image segmentation. Firstly, the two intensity fitting functions in the original local binary fitting (LBF) model are pre-estimated by using a local GMM-based intensity distribution estimator before curve evolution. The benefit of this pre-computation strategy is to avoid updating the fitting functions at each step of the curve evolution, and it also overcomes the initialisation problem of common gradient descent-based active contour models, i.e. the level-set function can be initialised as an arbitrary random matrix instead of a signed distance function in the proposed processing framework. Secondly, two processing ideas named global convex segmentation (GCS) method and split Bregman are introduced into the numerical implementation, where the role of GCS is to transform the proposed model into a simplified convex segmentation model, and the purpose of the split Bregman is to quickly output a convergent solution of the newly derived convex segmentation model in an alternate iterative format. Experimental results for synthetic and real images of different modalities with inhomogeneity or homogeneity validate the desired performances of the proposed method in terms of accuracy, robustness, and rapidity.

1 Introduction

Image segmentation is a critical task in many image processing and computer vision applications. Its purpose is to divide the input image into a number of meaningful regions whose inner pixels are homogenous or nearly homogenous with respect to certain features such as intensity, colour, and texture. The main challenge of image segmentation is that the image to be segmented is usually complex and is accompanied by noise, intensity inhomogeneity, texture, or disordered structure. In the past few decades, researchers at home and abroad have developed a variety of effective image-segmentation algorithms, of which the active contour model is the most promising one. The active contour model transforms the image-segmentation problem into a minimisation problem of the energy functional (used to specify the constraint relationship of the segmentation process). By minimising the energy functional, the evolution curve can move towards the boundary position of the target and output closed and smooth segmentation results at the convergence state. The level-set method (LSM) is an important part of the active contour family, which was originally proposed by Osher and Sethian [1]. Compared to explicit active contour models [2, 3], which utilise parametric equations to represent evolving contours, LSMs represent the evolving contours as the zero level set of a higher dimensional function, thus making them numerically stable and easily able to handle topological changes.

According to the image information contained in the energy functional, we can roughly divide the LSM into the following two categories: the edge-based models [3–5] and the region-based models [6–10]. The edge-based model uses the gradient information of the image to construct the driving force required for the evolution process. When the input image has a sharp gradient, such models can indeed output high-quality segmentation results. However, there are two prominent drawbacks associated with such models, i.e. high sensitivity to noise interference and strong dependence on curve initialisations. Moreover, they may suffer from serious boundary leakage problems at weak boundaries. Contrary to the edge-based models, the region-based models use regional statistics inside and outside the evolving contour to generate driving forces. As a result, they are more robust to noise and can output more accurate segmentation results on images with

weak boundaries. Besides, they are less dependent on the position and shape of the initial curve. One of the most successful region-based models is the Chan–Vese (CV) model [6], which has been widely used in binary phase segmentation with the assumption that each image region is statistically homogeneous. However, the homogeneity assumption cannot precisely describe the intensity distribution of region with intensity inhomogeneity. Thus, it often fails to segment the images with intensity inhomogeneity.

In order to overcome the segmentation difficulty caused by the intensity inhomogeneity, some local region-based segmentation models [11–13] have been proposed. These methods generally believe that the images with intensity inhomogeneity satisfy the assumption of homogeneity within a very small local region, that is, within a sufficiently small local image region, we can assume that the intensity of the image is approximately statistically uniform. Thus, by fitting the given image in the sense of local region rather than global region, they can segment the images with intensity inhomogeneity. For example, in [11], a local binary fitting (LBF) energy is defined over the neighbourhood of each image point, and the entire target boundary is obtained by minimising the integral of the LBF energy over the whole image. The LBF model achieves good segmentation performance in segmenting inhomogeneous images; however, like most existing active contour models, the LBF model is also very sensitive to the initial contour location, which to some extent holds back their practical applications. In addition to the aforementioned initialisation sensitivity problem, the LBF model has another obvious drawback, that is, it needs to update the values of the two fitting functions f_1 and f_2 in each iteration, which brings a serious computational burden.

In order to effectively solve the problems of the original LBF model mentioned above, this paper propose a new level-set segmentation model which is driven by local GMM [14] and split Bregman [15, 16]. Firstly, the intensity distribution functions f_1 and f_2 are derived using a local GMM-based intensity distribution estimator before curve evolution. The parameters of the intensity distributions therefore are pre-estimated, and the proposed model avoids the step of updating them at each iteration of curve evolution. The proposed model therefore overcomes the

initialisation problem of common gradient descent-based active contour models and significantly improves the computational speed. Secondly, two processing ideas named the global convex segmentation (GCS) method [17] and split Bregman are introduced into the numerical implementation of the new LBF model. The specific implementation details are as follows: (1) remove the level-set regularisation term in the total energy functional; (2) remove the Dirac coefficient to generate a simplified gradient descent flow with the same static solution as the original problem; (3) limit the range of the level-set function to a finite constant interval; (4) the original total variation (TV) norm [18] is modified as an edge indicator function weighted TV norm to obtain an output similar to the geodesic active contour (GAC) model [4]; and (5) the split Bregman method is applied to the newly generated convex minimisation problem. Under the influence of the optimisation logic of this paper, the proposed level-set model shows excellent processing performance in the segmentation applications of inhomogeneous images.

The remainder of this paper is organised as follows. Section 2 is a brief description of the background. Section 3 presents the proposed model and its corresponding implementation strategies. Section 4 validates the proposed model by extensive experiments and discussions. Finally, conclusions are drawn in Section 5.

2 Background

2.1 LBF model

In order to handle the image-segmentation problem caused by intensity inhomogeneity, Li *et al.* [11] proposed an active contour model based on LBF energy; the core idea of the LBF model is to define a local intensity fitting energy for a given point x . By introducing a kernel function, its energy functional can be represented by a level-set formulation as

$$\begin{aligned} E_x^{\text{LBF}}(\phi, f_1(x), f_2(x)) \\ = \lambda_1 \int_{\Omega} K_{\sigma}(x-y) |I(y) - f_1(y)|^2 H(\phi(y)) dy \\ + \lambda_2 \int_{\Omega} K_{\sigma}(x-y) |I(y) - f_2(y)|^2 (1 - H(\phi(y))) dy \end{aligned} \quad (1)$$

where x is a centre point in a given grey image I defined on Ω , λ_1 and λ_2 are two positive constants, K_{σ} is a kernel function with a localisation property that $K_{\sigma}(u)$ decreases and approaches zero as $|u|$ increases, $f_1(x)$ and $f_2(x)$ are two numbers that fit image intensities near the point x , H is the Heaviside function, and ϕ is a level-set function.

By extending the centre point x to the entire image area, the following fitting energy corresponding to the input image can be obtained:

$$\begin{aligned} E^{\text{LBF}}(\phi, f_1, f_2) \\ = \int_{\Omega} E_x^{\text{LBF}}(\phi, f_1(x), f_2(x)) dx \\ = \lambda_1 \int_{\Omega} \left(\int_{\Omega} K_{\sigma}(x-y) |I(y) - f_1(y)|^2 H(\phi(y)) dy \right) dx \\ + \lambda_2 \int_{\Omega} \left(\int_{\Omega} K_{\sigma}(x-y) |I(y) - f_2(y)|^2 (1 - H(\phi(y))) dy \right) dx \end{aligned} \quad (2)$$

In order to enhance the smoothness of the level-set evolution process, two regularisation schemes are introduced to ensure the stability of the level-set evolution. One is the curve length regularisation term $L(\phi)$. Its purpose is to reduce the influence of noise. The other is the level-set regularisation term $P(\phi)$ which is imposed on the whole level-set function. Under its constraints, the time-consuming level-set re-initialisation step that is widely used in the traditional LSMs is completely removed. In summary, the entire energy functional can be expressed as follows:

$$\Gamma^{\text{LBF}}(\phi, f_1, f_2) = E^{\text{LBF}}(\phi, f_1, f_2) + \mu L(\phi) + \nu P(\phi) \quad (3)$$

where μ and ν are two controlling parameters, and

$$L(\phi) = \int_{\Omega} \delta(\phi(x)) |\nabla \phi(x)| dx \quad (4)$$

$$P(\phi) = \int_{\Omega} \frac{1}{2} |\nabla \phi(x) - 1|^2 dx \quad (5)$$

Minimising the energy functional Γ^{LBF} with respect to ϕ by using the calculus of variation and replacing H and δ in (2) and (4) with H_{ϵ} and δ_{ϵ} , the following gradient descent flow can be obtained:

$$\begin{aligned} \frac{\partial \phi}{\partial t} = & -\delta_{\epsilon}(\phi)(\lambda_1 e_1 - \lambda_2 e_2) + \mu \delta_{\epsilon}(\phi) \operatorname{div} \left(\frac{\nabla \phi}{|\nabla \phi|} \right) \\ & + \nu \left(\nabla^2(\phi) - \operatorname{div} \left(\frac{\nabla \phi}{|\nabla \phi|} \right) \right) \end{aligned} \quad (6)$$

where

$$\begin{cases} e_1(x) = \int_{\Omega} K_{\sigma}(y-x) |I(y) - f_1(y)|^2 dy \\ e_2(x) = \int_{\Omega} K_{\sigma}(y-x) |I(y) - f_2(y)|^2 dy \end{cases} \quad (7)$$

with

$$\begin{cases} H_{\epsilon}(x) = \frac{1}{2} \left[1 + \frac{2}{\pi} \arctan \left(\frac{x}{\epsilon} \right) \right] \\ \delta_{\epsilon}(x) = \frac{1}{\pi} \cdot \frac{\epsilon}{\epsilon^2 + x^2} \end{cases} \quad (8)$$

and

$$\begin{cases} f_1(x) = \frac{K_{\sigma}(x)^* [H_{\epsilon}(\phi(x)) I(x)]}{K_{\sigma}(x)^* H_{\epsilon}(\phi(x))} \\ f_2(x) = \frac{K_{\sigma}(x)^* [1 - H_{\epsilon}(\phi(x)) I(x)]}{K_{\sigma}(x)^* [1 - H_{\epsilon}(\phi(x))]} \end{cases} \quad (9)$$

In actual calculation, the construction process of the local binary image ($\mu_1 e_1 - \mu_2 e_2$) is based on all the pixels in a local Gaussian window. This localisation property is the real reason for the LBF model to be able to segment inhomogeneous images. However, when the contour is located at a certain location where $\mu_1 e_1 = \mu_2 e_2$, the local image fitting force will be zero, which leads to the evolution process be trapped into certain local minima, thus the segmentation result has a strong correlation with the initial position of the curve.

2.2 Gaussian mixture model

In the field of image segmentation, GMM [14] is often used to model the probability distribution of the image region, and in particular to characterise the foreground and background intensity distributions of the image to be segmented. The basic principles and implementation details of GMM are briefly summarised as follows.

Consider a given vector valued image $I: \Omega \rightarrow \mathbb{R}^d$, where $\Omega \subset \mathbb{R}^n$ is the image domain and $d \geq 1$ is the dimension of the vector I . For grey-level images, $d = 1$, and for colour images, $d = 3$. Suppose that the image plane contains M approximately homogeneous regions and the total number of pixels is N , i.e. $I = \{x_i, i = 1, \dots, N\}$. Further, assume the intensity value of the i th region follows the Gaussian distribution with the attribute parameter $\theta_i = (\mu_i, \Sigma_i)$, $i = 1, \dots, M$, where μ_i and Σ_i are the mean and covariance matrices of the region, respectively, and its mathematical description is as follows:

$$p(I|\theta_i) = \frac{1}{(2\pi)^{n/2} |\sum_i|^{1/2}} \exp\left(-\frac{1}{2}(x_i - \mu_i)^T \sum_i^{-1} (x_i - \mu_i)\right), \quad i = 1, \dots, M \quad (10)$$

By using certain rules to mix the above M components, we can obtain the intensity distribution function of the entire image. In other words, the mixed probability distribution function of the image can be expressed as

$$p(I|\theta, w) = \sum_{i=1}^M w_i p(I|\theta_i) \quad (11)$$

where $\theta = (\theta_1, \dots, \theta_M)$ is a set of attribute parameters for all components, $w = (w_1, \dots, w_M)$ is a group of weighting coefficients, and w_i is the coefficient of the i th component, and we call it the prior probability of each component. These weighting coefficients satisfy the following constraints

$$\sum_{i=1}^M w_i = 1, \quad w_i > 0, \quad i = 1, \dots, M \quad (12)$$

Next, our task becomes to estimate the aforementioned unknown parameters $\{\theta, w\}$ so that (11) can obtain the maximum value.

For the parameter estimation problem of the GMM model, expectation–maximisation (EM) is the most commonly used algorithm. In this paper, we also use it to estimate the optimal parameter values of the GMM model. The EM algorithm consists of E-step and M-step. The role of E-step is to estimate the expected values of the unknown parameters and give the current parameter estimate, and the role of M-step is to re-estimate the distribution parameters so that the likelihood of the data is maximised, and then the expected estimate of the unknown variables is given.

Here, we represent all the parameters that need to be estimated as a mixture variable named $\Theta = \{\theta_1, \dots, \theta_M, w_1, \dots, w_M\}$, and let $\Theta^{(t)}$ denote the estimate of parameter Θ after the t th iteration. At the subsequent $(t+1)$ th iteration, the E-step calculates the following expected data log likelihood function:

$$LL(\Theta, \Theta^{(t)}) = \sum_{j=1}^N \sum_{i=1}^M \{ \log w_i p(x_j | \theta_i) \} p(i|x_j, \Theta^{(t)}) \quad (13)$$

where $p(i|x_j, \Theta^{(t)})$ represents the posterior probability that pixel x_j belongs to region i , which has the following calculation expression:

$$p(i|x_j, \Theta^{(t)}) = \frac{w_i^{(t)} p(x_j | \theta_i^{(t)})}{\sum_{m=1}^M w_m^{(t)} p(x_j | \theta_m^{(t)})} \quad (14)$$

Then, we use M-step to estimate the distribution parameter $\Theta^{(t+1)}$. By using the gradient descent method to solve the maximum value of (13), we can obtain the updated values of the prior probabilities and distribution parameters as follows:

$$w_i^{(t+1)} = \frac{1}{N} \sum_{j=1}^N p(i|x_j, \Theta^{(t)}) \quad (15)$$

$$\mu_i^{(t+1)} = \frac{\sum_{j=1}^N x_j p(i|x_j, \Theta^{(t)})}{\sum_{j=1}^N p(i|x_j, \Theta^{(t)})} \quad (16)$$

$$(\Sigma_i^{(t+1)})^2 = \frac{\sum_{j=1}^N x_j p(i|x_j, \Theta^{(t)}) (x_j - \mu_i^{(t+1)}) (x_j - \mu_i^{(t+1)})^T}{\sum_{j=1}^N p(i|x_j, \Theta^{(t)})} \quad (17)$$

The updated parameters obtained through the M-step are passed directly to the next E-step, and the process continues until it meets the predefined iteration conditions. In the image-segmentation

application of this paper, only the distribution of the foreground and background areas needs to be considered. Therefore, the value of M is 2.

3 Proposed method and its implementation strategies

3.1 Proposed method

In the previous description of the LBF model, we pointed out that the LBF model heavily depends on the position of the initial curve, which means that improper initialisation will bring wrong segmentation results. From (9), we can see that the values of the fitting functions f_1 and f_2 are directly related to the current level-set function, which means that we need to update the values of f_1 and f_2 at each step of the iteration process. This will undoubtedly increase the overall computational burden of the evolutionary process. In order to overcome the aforementioned computational overloading problem and improve the robustness of the LBF model to the initial curve, we propose the following local distribution fitting energy:

$$p(i|x_j, \Theta^{(t)}) = \frac{w_i^{(t)} p(x_j | \theta_i^{(t)})}{\sum_{m=1}^M w_m^{(t)} p(x_j | \theta_m^{(t)})} \quad (18)$$

where $M_1(\phi) = H(\phi)$ and $M_2(\phi) = 1 - H(\phi)$; h_1 and h_2 correspond to the local background and object distribution fitting functions, respectively. Using (16) in the way of local GMM to the input image, we can easily calculate μ_1 and μ_2 before contour evolution, which exactly correspond to h_1 and h_2 . By using a localised GMM, the intensity distribution of the background and foreground will be mixed together within the local neighbourhood of each image pixel.

The proposed model is similar in form to the LBF model. The only difference between the two models is that the proposed model uses different local fitting functions h_1 and h_2 , which are estimated by the local GMM (the word ‘local’ means that we only need to calculate the distribution parameters within the local region defined by the Gaussian kernel function). What needs to be emphasised here is that the estimation process is independent of the evolution process of the level-set function. This means that we can pre-calculate the local fitting functions h_1 and h_2 required by the proposed model before the evolution process begins. In other words, in the entire evolution of the level-set function, we do not need to update the values of h_1 and h_2 and always keep them constant. In addition, the pre-calculation of h_1 and h_2 essentially eliminates the need for user initialisation, i.e. level-set function can be initialised as a random matrix. Therefore, the proposed model overcomes the inherent initial curve sensitivity problem of the LBF model and many existing active contour models.

Next, we construct the functional energy of this paper by additionally introducing a certain number of regularisation energy terms (collectively refer to as $R(\phi)$) and integrate E_x^{LDF} over all the pixel locations:

$$\Gamma^{\text{LDF}}(\phi, h_1, h_2) = \int E_x^{\text{LDF}}(\phi, h_1(x), h_2(x)) dx + R(\phi) \quad (19)$$

Taking a similar approach to that of the LBF model, we can derive the gradient descent flow equation corresponding to (19):

$$\frac{\partial \phi}{\partial t} = -\delta_\epsilon(\phi)(\lambda_1 e_1^* - \lambda_2 e_2^*) + r(\phi) \quad (20)$$

where $r(\phi) = -(\partial R(\phi)/\partial(\phi))$, and

$$e_i^*(x) = \int K_\sigma(y-x) |I(x) - h_i(y)|^2 dy, \quad i = 1, 2 \quad (21)$$

3.2 Implementation strategies

Similar to the CV [6] model, the level-set segmentation model shown in (16) is also non-convex. According to the related knowledge of optimisation theory, we know that the non-convexity will not only affect the convergence speed of the model, but also cause the model to fall into local minimum (sometimes may correspond to wrong segmentation results).

In order to solve the problems caused by the non-convexity of the level-set models, Chan *et al.* [17] proposed the GCS method. The GCS method not only makes the model numerically easier to handle, but also makes the model not fall into a local minimum and thus more reliable. Subsequently, Goldstein *et al.* [15] proposed a convex and fast segmentation model by applying the GCS method and split Bregman method [16] to the CV model, which is called global convex CV model. However, as with the CV model, the globally convex CV model is mainly used to segment the images with intensity homogeneity in the target region, and it is powerless for the images with intensity inhomogeneity within the target area. In order to handle the images with intensity inhomogeneity better and faster, we combine the modified LBF model, the GCS method, and the split Bregman method together to build a new globally convex segmentation model, the proposed model can quickly and efficiently segment the images with intensity inhomogeneity.

The process includes the following two steps: (1) transforming the target functional into a GCS model and (2) minimising the newly generated model based on split Bregman.

3.2.1 Transforming the target functional into a GCS model: In accordance with Chan *et al.*'s [17] idea of transforming non convex function into global convex function, we first remove the level-set regularisation term in (6). Removing the level-set regularisation term from the equation is reasonable and does not affect the availability and reliability of the new model in practice. The results of the experimental part can prove this argument. The evolution equation after removing the level-set regularisation term is as follows:

$$\frac{\partial \phi}{\partial t} = \delta_e(\phi) \left((\lambda_2 m_2 - \lambda_1 m_1) + \mu \operatorname{div} \left(\frac{\nabla \phi}{|\nabla \phi|} \right) \right) \quad (22)$$

and without losing the generality, we set the value of parameter μ to 1.

According to the global convex segmentation idea of Chan *et al.* [17], we know that the following equation has the same static solution as (22).

$$\frac{\partial \phi}{\partial t} = (\lambda_2 m_2 - \lambda_1 m_1) + \operatorname{div} \left(\frac{\nabla \phi}{|\nabla \phi|} \right) \quad (23)$$

We now construct an energy functional whose gradient descent flow is exactly (23), and its expression is

$$E_{\text{new}}(\phi) = \int_{\Omega} |\nabla(\phi(x))| dx + \int_{\Omega} \phi(x)(\lambda_1 m_1(x) - \lambda_2 m_2(x)) dx \quad (24)$$

Therefore, the minimisation problem we need to solve is

$$\begin{aligned} \min E_{\text{new}}(\phi) \\ = \min \left(\int_{\Omega} |\nabla(\phi(x))| dx + \int_{\Omega} \phi(x)(\lambda_1 m_1(x) - \lambda_2 m_2(x)) dx \right) \end{aligned} \quad (25)$$

We note that the energy function shown in (25) is a homogeneous function of order one of ϕ , so it usually does not have a unique global minimum. This problem is caused by the non-uniqueness of the level-set representation. We can guarantee the global minimum by limiting the level-set function ϕ to a finite constant interval $[c_L, c_R]$, that is, $c_L \leq \phi \leq c_R$. Therefore, we further have

$$\min_{c_L \leq \phi \leq c_R} E_{\text{new}}(\phi) = \min_{c_L \leq \phi \leq c_R} \left(\int_{\Omega} |\nabla(\phi(x))| dx + \int_{\Omega} \phi(x)s(x) dx \right) \quad (26)$$

where $s(x) = \lambda_1 m_1(x) - \lambda_2 m_2(x)$.

Once the evolution process reaches the optimal state of ϕ , the final segmented image Ω_{binary} can be found by thresholding the level-set function using a threshold T which is located in interval (c_L, c_R) , that is

$$\Omega_{\text{binary}} = \Omega_f \cup \Omega_b = \{x | \phi(x) > T\} \cup \{x | \phi(x) \leq T\}, \quad T \in (c_L, c_R) \quad (27)$$

In addition, we also notice that the first energy term of (26) is just the traditional TV [18] norm: $TV(\phi) = \int_{\Omega} |\nabla(\phi(x))| dx = |\nabla \phi|_1$.

Similar to the conversion idea of [19], we modify the energy functional (26) to incorporate the edge information of the image. This is achieved by weighting the traditional TV norm as follows:

$$TV_g(\phi) = \int_{\Omega} g(|\nabla(I(x))|) |\nabla(\phi(x))| dx = |\nabla(\phi)|_g \quad (28)$$

where I is the input image and g is an edge indicator function defined by

$$g(x) = \frac{1}{1 + \kappa|x|^2} \quad (29)$$

where κ is a constant parameter, which is used to control the detail level of the final segmentation result.

Combining the previous description, we obtain the following energy functional, which is exactly the convex function that we need to minimise by adopting the split Bregman method:

$$\min_{c_L \leq \phi \leq c_R} E_{\text{new}}(\phi) = \min_{c_L \leq \phi \leq c_R} (|\nabla \phi|_g + \langle \phi, s \rangle) \quad (30)$$

where $\langle \phi, s \rangle = \int_{\Omega} \phi(x)s(x) dx$.

3.2.2 Minimising the newly generated model based on split Bregman: In order to use the split Bregman method to minimise the optimisation problem shown in (30), we need to introduce an auxiliary variable $\vec{d} = (d^r, d^b)$, and add a quadratic penalty function to weakly enforce the equality constraint $\vec{d} = |\nabla \phi|$. Thus (30) is transformed into the following unconstrained optimisation problem:

$$(\phi^*, \vec{d}^*) = \arg \min_{c_L \leq \phi \leq c_R, \vec{d}} |\vec{d}|_g + \langle \phi, s \rangle + \frac{\theta}{2} \|\vec{d} - \nabla \phi\|^2 \quad (31)$$

The Bregman iteration is then used to strictly enforce the constraint $\vec{d} = |\nabla \phi|$, which leads to the following optimisation problem:

$$(\phi^{k+1}, \vec{d}^{k+1}) = \arg \min_{c_L \leq \phi \leq c_R, \vec{d}} |\vec{d}|_g + \langle \phi, s \rangle + \frac{\theta}{2} \|\vec{d} - \nabla \phi - \vec{b}^k\|^2 \quad (32)$$

where \vec{b}^{k+1} is updated according to the formula:

$$\vec{b}^{k+1} = \vec{b}^k + \nabla \phi^{k+1} - \vec{d}^{k+1} \quad (33)$$

Keeping \vec{d} fixed, and minimising the energy functional shown in (32) with respect to ϕ , we derive the corresponding Euler-Lagrange equation:

$$\Delta \phi = \frac{s}{\theta} + \nabla \cdot (\vec{d} - \vec{b}), \quad \phi \in (c_L, c_R) \quad (34)$$

Here, we use the central and backward difference schemes to solve the Laplacian and divergence operators in (34) respectively:

$$\begin{cases} P_{i,j} = d_{i-1,j}^x - d_{i,j}^x + d_{i,j-1}^y - d_{i,j}^y - (b_{i-1,j}^x - b_{i,j}^x + b_{i,j-1}^y - b_{i,j}^y) \\ Q_{i,j} = \frac{1}{4}(\phi_{i-1,j} + \phi_{i+1,j} + \phi_{i,j-1} + \phi_{i,j+1} - \frac{s}{\theta} + P_{i,j}) \\ \phi_{i,j} = \max \{ \min \{ Q_{i,j}, c_R \}, c_L \} \end{cases} \quad (35)$$

Similarly, keeping ϕ fixed, and minimising (28) with respect to \vec{d} , we obtain

$$\vec{d}^{k+1} = \text{shrink}_g\left(\vec{b}^k + \nabla\phi^{k+1}, \frac{1}{\theta}\right) = \text{shrink}\left(\vec{b}^k + \nabla\phi^{k+1}, \frac{g}{\theta}\right) \quad (36)$$

where $\text{shrink}(x, y)$ is the shrinkage operator [20] defined as

$$\text{shrink}(x, y) = \begin{cases} \frac{x}{|x|} \max(|x| - y, 0), & x \neq 0 \\ 0, & x = 0 \end{cases} \quad (37)$$

4 Experimental results and discussions

The performance of the proposed method has been validated in image-segmentation experiments on a wide variety of images, including synthetic images, medical images and infrared images. All experiments are implemented by Matlab R2012a on a computer with Intel Core i7 2.3 GHz CPU, 8G RAM, and Windows 7 operating system. For the following parameters, we use the same values for all experiments, i.e. $\lambda_1 = 1$, $\lambda_2 = 1$, $c_L = 0$, $c_R = 1$, $\theta = 1$, $\Delta t = 0.2$ (time step), $T = 0.004$. In addition, when estimating the distribution parameters of the local GMM model, we set the size of the local image region as 11 by 11. In each subsequent set of experiments, we will give the two mean images corresponding to the local GMM. What needs to be specifically stated here is that the methods involved in the comparison and the proposed method all belong to the pure data-driven type, and do not adopt any form of shape priors.

In order to test the generalisation ability of the proposed model, we adopted a method of randomly selecting the test images. Some of these images come from the literatures on image segmentation, and some come from the internet. These images are weakly related to each other.

In addition, to quantitatively evaluate the segmentation results, we use four region overlap metrics, which are defined as follows:

$$JS = \frac{N(S_{\text{reference}} \cap S_{\text{test}})}{N(S_{\text{reference}} \cup S_{\text{test}})} \quad (\text{jaccardsimilarity [21]}) \quad (38)$$

$$DSC = \frac{2N(S_{\text{reference}} \cap S_{\text{test}})}{N(S_{\text{reference}}) + N(S_{\text{test}})} \quad (\text{dicesimilaritycoefficient [22]}) \quad (39)$$

$$FPR = \frac{N(S_{\text{reference}} \setminus S_{\text{common}})}{N(S_{\text{reference}})} \quad (\text{falsepositiveratio}) \quad (40)$$

$$FNR = \frac{N(S_{\text{test}} \setminus S_{\text{common}})}{N(S_{\text{test}})} \quad (\text{falsenegativeratio}) \quad (41)$$

where ‘ \cap ’ and ‘ \cup ’ represent the intersection and union of two regions, respectively, S_{test} , $S_{\text{reference}}$ and S_{common} are the output region of the segmentation algorithm, the ground-truth and the common part of two regions, respectively, $N(\cdot)$ represents the number of pixels in the enclosed set. Obviously, the closer the JS and DSC values to 1, and the FPR and FNR values to 0, the better the segmentation results.

Next, we will carry out our experiments from the following three aspects: accuracy, robustness, rapidity.

4.1 Accuracy

We will verify the accuracy of our method from two aspects: inhomogeneous image segmentation and homogenous image segmentation.

Fig. 1 shows the verification experiments for inhomogeneous image-segmentation applications. The test image consists of two X-ray images of vessels, and a real image of a T-shaped object. All of them are typical images with intensity inhomogeneity. In order to fully demonstrate the superiority of the proposed model in terms of segmentation accuracy, we compare it with several other classical segmentation models, in which the level-set segmentation methods are GAC model [4], novel generalised gradient vector flow (NG-GVF) snake model [5], CV model [6], region-based active contour model via local similarity factor (RLSF) [8], Kullback-Leibler divergence and multi-scale local binary fitting-driven (KL-MLBF) active contour model [9], local pre-fitting energy-driven (LPFE) active contours model [10], and the traditional non-level-set segmentation methods include Nobuyuki Otsu's (OTSU) algorithm [23], pulse coupled neural networks (PCNN) algorithm [24] and general GMM (g-GMM) algorithm [14]. Fig. 1 shows the results of this set of comparison experiments, where Fig. 1a is the input images and the initial contours required for the level-set-based segmentation methods, Figs. 1b and c are the local fitting functions h_1 and h_2 , respectively, and Figs. 1d to m are the segmentation results by using the GAC, NG-GVF, CV, RLSF, KL-MLBF, LPFE, OTSU, PCNN, g-GMM and our models respectively. In order to be consistent with the expression form of traditional non-level-set segmentation methods, we use two valued images here to represent the segmentation results corresponding to the final evolution contours of the LSMs. It is easy to visually find through this set of experiments that the traditional segmentation methods are difficult to obtain ideal segmentation results, and they all have different degrees of segmentation errors, on the contrary, our method outputs satisfactory segmentation results on all of these challenging images. Table 1 presents the aforementioned four region overlap metrics in a quantitative manner, by comprehensively comparing these data, we can clearly find out that our method does obtain the optimal segmentation performance.

Fig. 2 shows a set of comparison experiments for homogenous image segmentation. The input images shown in Fig. 2a have approximately homogeneous target and background characteristics. In this set of experiments, the proposed method is only compared with the literature that belongs to the level-set segmentation type and published in recent years. When initialising the evolution process the level-set evolution process of this set of experiments, we take the same form in which the rectangular curve intersects only a small part of the target region, and the visual effect is shown in Figs. 2a. Figs. 2b and c show the local fitting functions h_1 and h_2 , respectively. Since the segmentation methods of this set of comparison experiments are all of level-set type, when describing the final convergence result, we adopt the curve expression form commonly used by the LSM, and the pixels enclosed by the final curve is the target region corresponding to the input image. Figs. 2d-h are the final segmentation results based on the aforementioned expression logic, which correspond to NG-GVF, RLSF, KL-MLBF, LPFE and our models, respectively. By carefully analysing the convergence curves of this set of experiments, we find that even without using the regional overlap measure to quantitatively prove the final segmentation results, we can easily draw the following conclusion: Our method is also very adaptable to homogeneous images, and the other four methods involved in the comparison show different types of errors. From this set of seemingly simple images, we once again confirm the adaptability of the proposed method to different types of images.

4.2 Robustness

The robustness here includes two aspects. One is the robustness to contour initialisation, i.e. when different (represented by the difference of position and shape of the initial contour) initialisations are adopted, whether the evolution process outputs the same and accurate segmentation results? The other is the

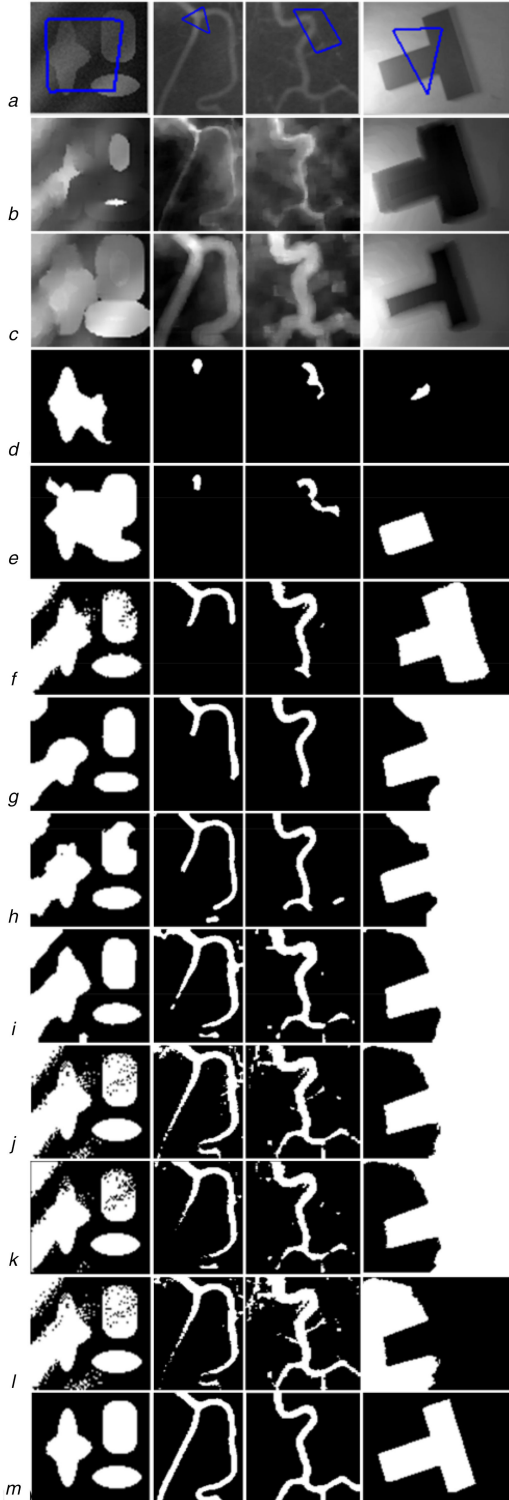


Fig. 1 Set of comparison experiments used to verify the accuracy of different segmentation algorithms on inhomogeneous image-segmentation applications
Row (a) is the input images and the initial contours required for the level-set-based segmentation methods, rows (b) and (c) are the local fitting functions h_1 and h_2 , respectively, and rows (d) to (m) are the segmentation results by using the GAC, NG-GVF, CV, RLSF, KL-MLBF, LPFE, OTSU, PCNN, g-GMM, and our models, respectively

robustness to natural interference (background information of real-life image data), i.e. when the input real-life image contains different degrees of background interference, can the algorithm suppress it and successfully extract the foreground target of the image?

Fig. 3 shows a set of comparison experiments for the robustness to contour initialisation. All the test data are medical images (as shown in the first row of Fig. 3), in which the vascular targets have different degrees of intensity inhomogeneity. For all these experiments, each level-set function is initialised as a numerical matrix containing pseudorandom values drawn from the standard uniform distribution on the open interval (0, 1). Since each run of

the computer program generates different random data, in Fig. 3, we omit the two-dimensional or three-dimensional representation of the initial level-set function. The second to third rows of Fig. 3 are the local fitting functions h_1 and h_2 , respectively. Here, the proposed method is only compared with the following level-set segmentation models: LBF, RLSF, KL-MLBF, LPFE. Since we are unable to generate the coordinate sequence required for the initialisation of NG-GVF under the aforementioned random matrix initialisation mode, we have to delete NG-GVF from the comparison method family of this group of experiments. Their segmentation results correspond to the fourth to seventh rows of Fig. 3, respectively. The segmentation results of our method are

Table 1 Region overlap metrics of different algorithms, where ‘No. 1’ to ‘No. 4’ are the serial numbers of the images shown in row (a) of Fig. 1 from left to right

Image	Algorithm	Metrics (JS-DSC-FPR-FNR)		
No. 1	GAC	0.3650	0.5348	0.5805
	NG-GVF	0.7219	0.8385	0.0183
	CV	0.6563	0.7925	0.0643
	RLSF	0.6122	0.7595	0.2197
	KL-MLBF	0.6888	0.8157	0.0994
	LPFE	0.6435	0.7831	0.0643
	OTSU	0.6568	0.7929	0.0450
	PCNN	0.6176	0.7636	0.1527
	g-GMM	0.6495	0.7875	0.0513
	our method	0.9783	0.9890	0.0110
No. 2	GAC	0.0551	0.1044	0.9446
	NG-GVF	0.0524	0.0996	0.9475
	CV	0.3819	0.5527	0.6094
	RLSF	0.4564	0.6268	0.5248
	KL-MLBF	0.6112	0.7587	0.3820
	LPFE	0.5925	0.7441	0.2774
	OTSU	0.6220	0.7669	0.1966
	PCNN	0.5492	0.7090	0.3952
	g-GMM	0.6212	0.7663	0.2922
	our method	0.9468	0.9727	0.0283
No. 3	GAC	0.1059	0.1915	0.8886
	NG-GVF	0.1106	0.1992	0.8773
	CV	0.5547	0.7135	0.3936
	RLSF	0.5021	0.6685	0.4781
	KL-MLBF	0.6317	0.7743	0.3623
	LPFE	0.6793	0.8090	0.1902
	OTSU	0.6702	0.8025	0.1302
	PCNN	0.6363	0.7777	0.2697
	g-GMM	0.5997	0.7497	0.0720
	our method	0.9553	0.9772	0.0232
No. 4	GAC	0.0050	0.0100	0.9948
	NG-GVF	0.3424	0.5101	0.6563
	CV	0.6447	0.7840	0.1358
	RLSF	0.0092	0.0182	0.9795
	KL-MLBF	0.0028	0.0056	0.9938
	LPFE	0.0134	0.0265	0.9688
	OTSU	0.0129	0.0254	0.9704
	PCNN	0.0184	0.0362	0.9581
	g-GMM	0.0121	0.0240	0.9724
	our method	0.9514	0.9751	0.0260

shown in the eighth row of Fig. 3. What needs to be specifically explained here is that each row starting from the fourth row is split into three sub-rows, which correspond to different random initialisations. From the segmentation results shown in the fourth to eighth rows, we can intuitively see that the comparison models outside the proposed method all output wrong segmentation results under random initialisation mode. It is particularly obvious that the segmentation results of models RLSF and KL-MLBF both show the characteristics of spot discontinuity, which is far from the correct segmentation results. On the contrary, our model outputs almost the same correct segmentation results. This fully proves that the proposed model is completely independent of initialisation, i.e. it is very robust to initialisation.

Next, we will present another set of comparison experiments for real-life image segmentation, through which we can indirectly verify the performance of these methods in real-life image background interference suppression. Since the proposed model does not contain any form of description and modeling unit for colour features, we only consider the intensity information of the pixels. Therefore, when segmenting real-life images (colour images), the input images actually involved in the operation are the grey versions of the real-life images. In addition, the family of

comparison methods here is as follows: LBF, RLSF, KL-MLBF and LPFE. The reason why the NG-GVF model of edge type is removed from the family of comparison methods here is that the background of this set of input images (a set of real-life images from the BSDS500 database and shown in Fig. 4a) contains a large number of smooth region blocks. At the same time, the purpose of doing so is to enhance the fairness and scientificity of the comparison experiment. The initialisation (as shown in Fig. 4a) here has the following common feature: The initial curve consists of a cluster of circles that cover almost the entire image plane. The purpose of this is to embed the background interference information as much as possible into the level-set evolution process in order to fully test the background suppression ability of the algorithm. Rows (b) to (c) of Fig. 4 are still the two fitting functions h_1 and h_2 (both are calculated from the grey version of the image data) output by the local GMM modeling process. Rows (d) to (h) are the segmentation results by using LBF, RLSF, KL-MLBF, LPFE and our models respectively. By visually observing these segmentation results, we can easily draw the following conclusion: under the initialisation mode that the initial curve contains a large number of background information, all the other models involved in the comparison output different types of error

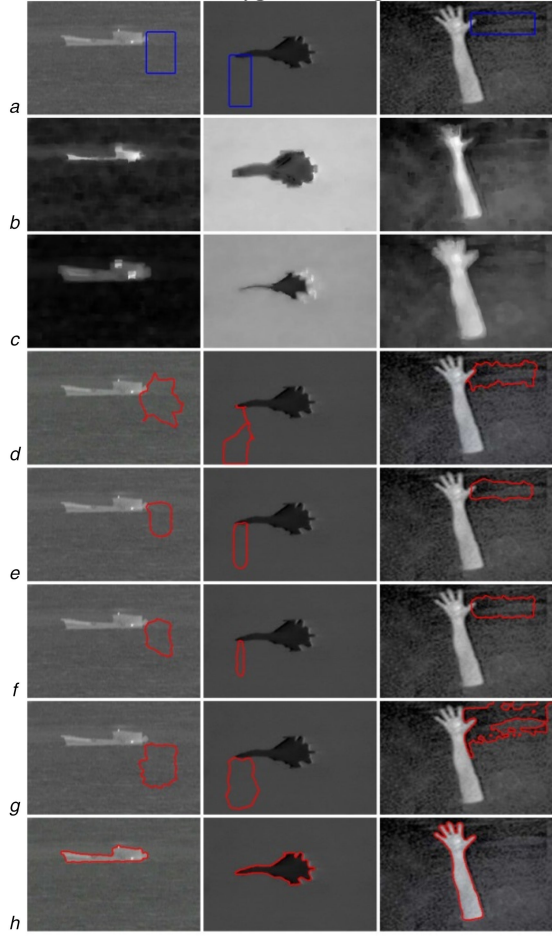


Fig. 2 Set of comparison experiments on segmentation accuracy metrics for homogeneous image-segmentation applications

Row **(a)** is the input images and the initial contours, rows **(b)** and **(c)** are the local fitting functions h_1 and h_2 , respectively, and rows **(d) to (h)** are the segmentation results by using the NG-GVF, RLSF, KL-MLBF, LPFE, and our models, respectively

results, while the proposed model output correct segmentation results, which fully illustrates the proposed model is also very adaptable to real image-segmentation applications.

4.3 Rapidity

The rapidity of the proposed model can be reflected by the number of iterations and the CPU time required to complete the entire evolution process. It is well known that the comparison of the metric of rapidity is meaningful only when the segmentation results of the models participating in the comparison are correct. In view of this, when setting the initial curve, we will choose the most advantageous initialisation forms for the comparison models. Since the proposed method is a direct extension of the original LBF model, in this section, we only compare it with the LBF model to quantitatively and intuitively reflect the acceleration characteristics of the proposed model under the simplified family of comparison methods. Fig. 5 shows the results of our model and LBF model using the same initial contours, where the first row shows the original images (a real and three synthetic images) along with initial contours, the second and third rows are the local fitting functions h_1 and h_2 , respectively, and the fourth and fifth rows are the segmentation results of LBF model and our model, respectively. From the final convergence curves, we can clearly see that both models output correct segmentation results. The corresponding rapidity metrics for this set of experiments are shown in Table 2, and the sizes of these images are also shown under the image numbers. Since the efficient split Bregman method is used to solve the energy minimisation problem corresponding to our segmentation model, the CPU time and number of iterations required for the evolution process are greatly reduced. This

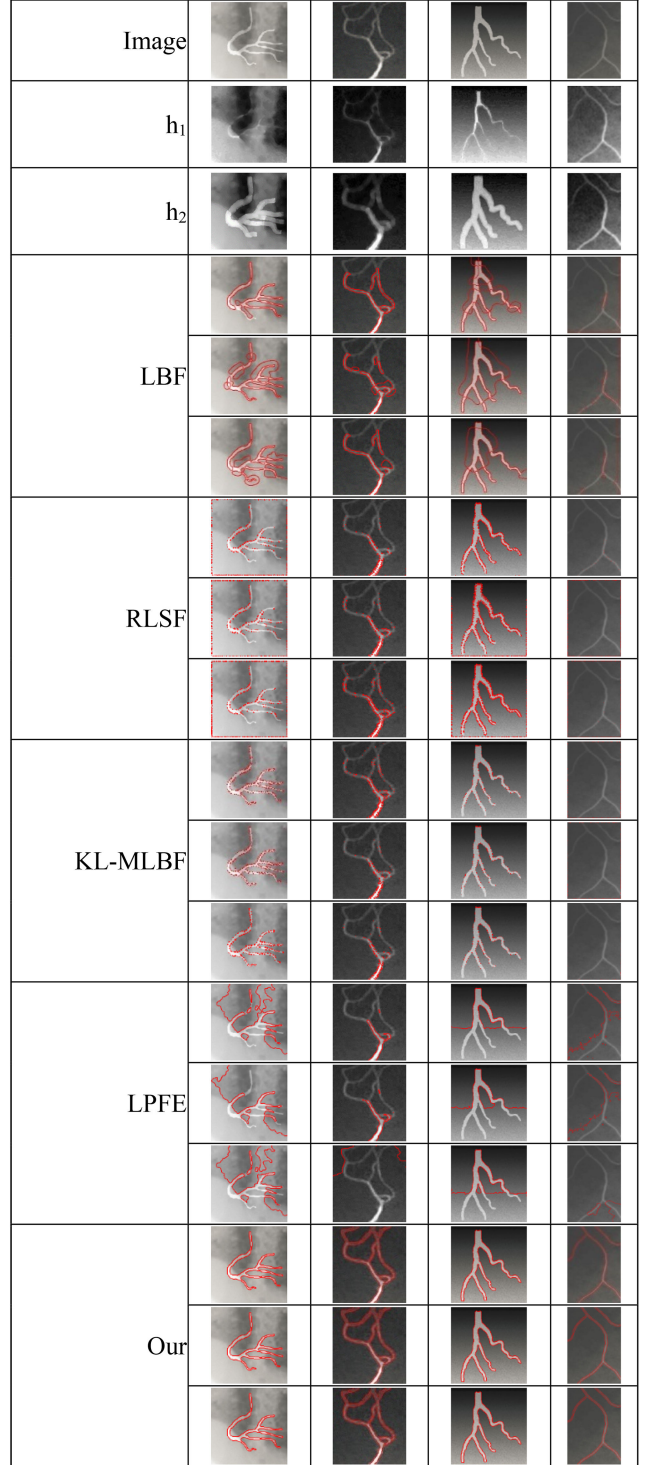


Fig. 3 Set of comparison experiments used to verify the robustness of our model and other models under different initialisations. The first row is the input images with intensity inhomogeneity; the second to third rows are the local fitting functions h_1 and h_2 , respectively, and the fourth to eighth rows are the segmentation results by using the LBF, RLSF, KL-MLBF, LPFE and our models respectively

demonstrates the significant advantage of our model in terms of computational efficiency.

5 Conclusions

In this paper, an effective image-segmentation method based on local GMM and split Bregman iteration is proposed in the framework of a level set, which achieves excellent performance in the segmentation applications of inhomogeneous images. Our method first estimates the two intensity fitting functions in the



Fig. 4 Set of comparison experiments for real-life image-segmentation applications (a)–(h)

original LBF model by using local GMM before the curve evolution process. The benefits of this approach are reflected in the following two aspects: one is that we do not need to update the two intensity fitting functions in every step of evolution process, which greatly reduces the time overhead of the evolution process; another is that the level-set function can be initialised as any form of the random number matrix, which completely overcomes the initialisation problem that is difficult to avoid by traditional LSMs, i.e. the segmentation result is highly correlated with initialisation. In the numerical implementation stage, we introduce the two ideas of GCS and split Bregman into our processing flow. Under the combined effect of these two optimisation strategies, the evolution speed of the proposed model has been greatly improved. The experimental results show that the proposed model shows excellent performance in terms of accuracy, rapidity, and robustness. In future research, we will further seek other numerical implementation strategies that can improve the performance of the segmentation models.

6 Acknowledgments

This work is supported by the Project of the Fundamental Research Funds for the Central Universities under Grant No. ZYGX2018J079. The authors would like to thank the anonymous reviewers for their valuable comments and advices.

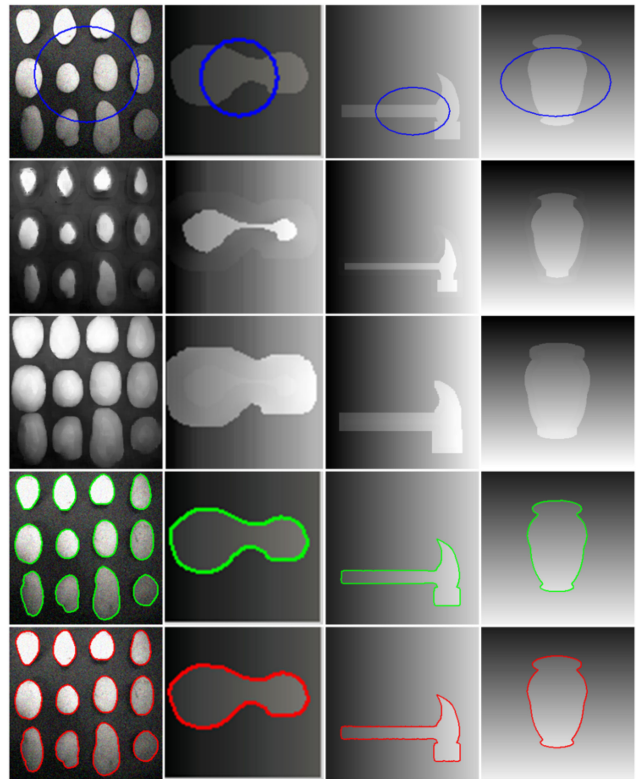


Fig. 5 Comparison of our model with the LBF model for rapidity

Table 2 Comparison of rapidity metrics for the images in Fig. 5 in the same order. The description format of the metrics is iteration number (CPU time (s))

	LBF model	Our model
image no. 1 (204×204)	275 (18.311)	42 (4.289)
image no. 2 (88×85)	106 (3.326)	16 (0.717)
image no. 3 (256×256)	237 (13.434)	36 (2.669)
image no. 4 (256×256)	154 (8.437)	24 (1.853)

7 References

- [1] Osher, S., Sethian, J.A.: ‘Fronts propagating with curvature-dependent speed: algorithms based on Hamilton-Jacobi formulations’, *J. Comput. Phys.*, 1988, **79**, (1), pp. 12–49
- [2] Kass, M., Witkin, A., Terzopoulos, D.: ‘Snakes: active contour models’, *Int. J. Comput. Vis.*, 1988, **1**, (4), pp. 321–331
- [3] Xu, C., Prince, J.L.: ‘Snakes, shapes, and gradient vector flow’, *IEEE Trans. Image Process.*, 1998, **7**, (3), pp. 359–369
- [4] Caselles, V., Kimmel, R., Sapiro, G.: ‘Geodesic active contours’, *Int. J. Comput. Vis.*, 1997, **22**, (1), pp. 61–79
- [5] Zhu, S., Gao, R.: ‘A novel generalized gradient vector flow snake model using minimal surface and component-normalized method for medical image segmentation’, *Biomed. Signal Process. Control.*, 2016, **26**, pp. 1–10
- [6] Chan, T.F., Vese, L.A.: ‘Active contours without edges’, *IEEE Trans. Image Process.*, 2001, **10**, (2), pp. 266–277
- [7] Ronfard, R.: ‘Region-based strategies for active contour models’, *Int. J. Comput. Vis.*, 1994, **13**, (2), pp. 229–251
- [8] Niu, S., Chen, Q., Sisternes, L., et al.: ‘Robust noise region-based active contour model via local similarity factor for image segmentation’, *Pattern Recognit.*, 2017, **61**, pp. 104–119
- [9] Liu, L., Cheng, D., Tian, F., et al.: ‘Active contour driven by multi-scale local binary fitting and Kullback-Leibler divergence for image segmentation’, *Multimedia Tools Appl.*, 2017, **76**, (7), pp. 10149–10168
- [10] Ding, K., Xiao, L., Weng, G.: ‘Active contours driven by local pre-fitting energy for fast image segmentation’, *Pattern Recognit. Lett.*, 2018, **104**, pp. 29–36
- [11] Li, C., Kao, C.-Y., Gore, J.C., et al.: ‘Implicit active contours driven by local binary fitting energy’. IEEE Conf. on Computer Vision and Pattern Recognition, 2007
- [12] Wang, L., He, L., Mishra, A., et al.: ‘Active contours driven by local Gaussian distribution fitting energy’, *Signal Process.*, 2009, **89**, (12), pp. 2435–2447
- [13] Zhang, K., Song, H., Zhang, L.: ‘Active contours driven by local image fitting energy’, *Pattern Recognit.*, 2010, **43**, pp. 1199–1206
- [14] McLachlan, G., Peel, D.: ‘Finite mixture models’, (John Wiley & Sons, New York, 2000)
- [15] Goldstein, T., Osher, S.: ‘The split Bregman method for L1 regularized problems’, *SIAM J. Imaging Sci.*, 2009, **2**, (2), pp. 323–343

- [16] Bregman, L.: ‘The relaxation method of finding the common points of convex sets and its application to the solution of problems in convex optimization’, *USSR Comput. Math. Phys.*, 1967, **7**, pp. 200–217
- [17] Chan, T.F., Esedoglu, S., Nikolova, M.: ‘Algorithms for finding global minimizers of image segmentation and denoising models’, *SIAM J. Appl. Math.*, 2006, **66**, (5), pp. 1632–1648
- [18] Rudin, L., Osher, S., Fatemi, E.: ‘Nonlinear total variation based noise removal algorithms’, *Physica D*, 1992, **60**, pp. 259–268
- [19] Bresson, X., Esedoglu, S., Vandergheynst, P., et al.: ‘Fast global minimization of the active contour/snake model’, *J. Math. Imaging Vis.*, 2007, **28**, (2), pp. 151–167
- [20] Goldstein, T., Bresson, X., Osher, S.: ‘Geometric applications of the split Bregman method: segmentation and surface reconstruction’, *J. Sci. Comput.*, 2010, **45**, pp. 272–293
- [21] Zheng, Q., Lu, Z., Yang, W., et al.: ‘A robust medical image segmentation method using KL distance and local neighborhood information’, *Comput. Biol. Med.*, 2013, **43**, pp. 459–470
- [22] Vovk, U., Pernus, F., Likar, B.: ‘A review of methods for correction of intensity inhomogeneity in MRI’, *IEEE Trans. Med. Imaging*, 2007, **26**, (3), pp. 405–421
- [23] Otsu, N.: ‘A threshold selection method from gray-level histograms’, *IEEE Trans. Syst. Man Cybern.*, 1979, **9**, (1), pp. 62–66
- [24] Kuntimad, G., Ranganath, H.S.: ‘Perfect image segmentation using pulse coupled neural networks’, *IEEE Trans. Neural Netw.*, 1999, **10**, (3), pp. 591–598